Research on Engineering Structures & Materials
www.jresm.org

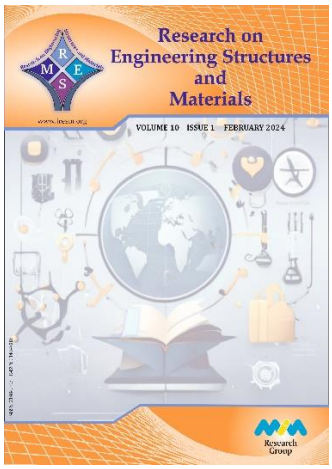

Corrosion behavior of fiber laser welded Ti-6Al-4V alloy rods with different pH and temperature in 0.9 wt% NaCl medium

Arife Kübra Yontar, Sinem Çevik

Online Publication Date: 30 October 2023
URL: http://www.jresm.org/archive/resm2023.39ma0821rs.html
DOI: http://dx.doi.org/10.17515/resm2023.39ma0821rs

Journal Abbreviation: *Res. Eng. Struct. Mater.*

To cite this article
Yontar AK, Cevik S. Corrosion behavior of fiber laser welded Ti-6Al-4V alloy rods with different pH and temperature in 0.9 wt% NaCl medium. *Res. Eng. Struct. Mater.*, 2024; 10(2): 537-557.

Research on Engineering Structures & Materials
www.jresm.org

Research Article

Corrosion behavior of fiber laser welded Ti-6Al-4V alloy rods with different pH and temperature in 0.9 wt% NaCl medium

Arife Kübra Yontar [*1,3,a], Sinem Çevik [1,2,b]

[1]*Department Mechanical and Metal Technologies, Ondokuz Mayis University, Samsun, Turkey*
[2]*Department of Metallurgical and Materials Engineering, Ondokuz Mayıs University, Samsun, Turkey*
[3]*Department of Nanoscience and Nanotechnology, Ondokuz Mayis University, Samsun, Turkey*

Article Info

Article history:

Received 21 Aug 2023
Accepted 30 Oct 2023

Keywords:

Ti-6Al-4V alloys;
Fiber laser welding;
Corrosion resistance;
NaCl solution;
Weight changes

Abstract

The corrosion resistance of laser welded samples was carried out in a shaken incubator in body-simulated liquid environments and kept at pH3-5 and 25-50°C conditions for 24 hours. It was determined that acicular α' martensite structures were formed in the fusion regions and these structures increased the hardness of the alloy by 20% compared to the base metal. The welded samples had the highest tensile strength of 144 MPa. Weight changes after the corrosion test were calculated and the highest weight loss was found to be 0.0025 g for the sample with an initial weight of 4.1394 g. TiO_2 oxides and {1 0 0} and {1 1 1} chamber-shaped salt crystals were formed larger and more intensely in the fusion zones than the base metal. Dental metallic implant welding with fiber laser will have higher corrosion resistance in oral use with different temperature and pH environments compared to screw joints.

1. Introduction

Titanium and its alloys have become very popular in biomaterial production with their superior properties. Ti-6Al-4V alloy has been a very common titanium alloy as an implant material [1–6]. The high preference for Ti-6Al-4V alloy as a biomaterial is due to high corrosion and abrasion resistance, low density, biocompatibility, high tensile strength and hardness properties. Its high corrosion resistance and biocompatibility are thanks to the thin oxide (TiO_2) layer formed on the outer surface of the metal due to titanium contact with oxygen [7–13]. These TiO_2, and TiO_3 layers formed on the surface may lose their properties by being affected by some environmental factors. The most important of these factors are temperature, pH and concentrations of fluoride, sodium and chlorine in the environment. Cl- or Na- ions can penetrate the surface and form an unstable layer, making re-passivation more difficult [14]. In addition, the difference that occurs between the titanium phases also makes a difference in the homogeneity of the oxide layer growth. Titanium and its alloys can corrode due to physical (stress, abrasion, forces, etc.) and chemical (acidic food and beverages, toothpaste, etc.) variable effects during their use in the body environment. Apart from these, heat treatments and applications also affect the corrosion properties of the metal because of the microstructure changes [15–20]. For this reason, it is critical for engineering and health applications to examine the effects of temperature and pH external factors on the welded parts of the Ti-6Al-4V alloys. It is desired that the metallic biomaterials to be used in the body or mouth be biocompatible and should not be corroded. As a result, titanium alloys with good corrosion resistance and

*Corresponding author: kubra.demirbas@omu.edu.tr
[a] orcid.org/0000-0003-1486-9332; [b] orcid.org/0000-0002-3506-7892
DOI: http://dx.doi.org/10.17515/resm2023.39ma0821rs

biocompatibility are used to make implants. Titanium and its alloys are generally used in acidic environments, especially in the mouth, drinking water and pool pipes, industrial coating boilers, etc. They can corrode in environments containing chloride ions. In such environments with high chloride ion concentrations, corrosion attacks occur more and cause alloy corrosion. Although the Ti-6Al-4V alloy is normally corrosion resistant, it can erode fast in hostile situations that dissolve the protective oxide layer. Titanium, on the other hand, can only be protected against corrosion assaults if a stable and continuous surface layer is formed on the Ti-6Al-4V alloy [21, 22]. Various surface treatments are carried out to increase the osseointegration properties and corrosion resistance of the implants. These methods include coating, laser surface roughening, electrochemical treatment, and thermal spraying.

Titanium alloys have a highly reactive chemical structure and their high melting points make it difficult to weld them. When the temperature exceeds 400 °C during welding, various gases such as oxygen, hydrogen and nitrogen can be easily absorbed on the surface, causing metallurgical defects to appear in the welding region. The ductility of titanium alloys decreases as they absorb intermediate elements such as oxygen, nitrogen and hydrogen onto their surfaces. Moreover, oxygen and nitrogen are powerful stabilizers in Ti-6Al-4V alloys and promote martensitic' development, resulting in brittle damage in the weld zone or surface. The creation of an oxygen-enriched outer layer known as the -case as a result of oxygen diffusion is difficult to manage. In order to weld titanium alloys, several fusion welding processes such as gas tungsten arc welding, gas metal arc welding, plasma arc welding, electron beam welding, and laser beam welding are employed [23–26]. However, the most effective joining method known is the fiber laser welding method. Fiber laser welding is a joining method that increases the production of metal materials. Although the fiber laser welding method increases the mechanical strength of metals, it can reduce their corrosion resistance. The fiber laser welding method creates a narrow welding seam due to its low energy density and adjustable heat input properties. For this reason, errors such as thermal stresses and micro-cracks in the welding zone and the heat-affected zone occur at very low rates [27–30]. Since the welding speed is faster than other welding methods in laser welding applications, the heat input occurring in the metal during the welding process is lower. Low heat input increases the cooling rate in the fusion zone, which causes the microstructure formed in the fusion zone to differ from the microstructure of the base metal. Changes in the microstructure of the metal after welding cause the behavior of the metal to change against corrosive effects [31–35]. Although Ti-6Al-4V can be successfully welded by the fiber laser method, a decrease in corrosion resistance may occur due to the following reasons; large dislocations, Fe element migration near grain boundaries and grains becoming coarser, β phase separation, increase in the number of anion vacancies, alpha exponent(α/) in the fusion region [36]. Ti-6Al-4V alloy corrosion resistance and high-temperature application are primarily determined by its microstructure, phase distribution, and finishing heat treatment parameters. There are three types of phase-dependent microstructures: (1) natural grainy layered structure (where α + β → β transformation occurs) that occurs after a gradual cooling or heat treatment above the β-trans temperature, i.e. Tβ; (2) fine coaxial (spherical) structure formed following deformation in the binary phase of the α + β field (below Tβ) where the α-phase is propagates in the β-matrix, and (3) bimodal microstructure comprised of primary α- in β grains phase and thin-layered α + β colonies [37].

Various corrosion tests have already been carried out on implant materials and titanium alloys in the literature, using methods such as open circuit potential (OCP), potentiodynamic and potentiostatic tests, and electrochemical impedance spectroscopy (EIS) [38–40]. Again, in these studies, corrosion behavior was investigated by using 0.9 wt wt% NaCl, Kroll or Hank solutions [41–44]. However, there are currently no studies carried

out by creating a naturally corrosive environment after fiber laser welding of Ti-6Al-4V (Gr5) alloys in rod form. The corrosion properties of implants that are used in the mouth and that have been treated with fiber laser welding are very important. The changes in the surface of the source area of the acidic environments they are exposed to during eating and drinking are a situation that needs to be examined. For this reason, the joint ability of this Gr 5 alloy by fiber laser welding method and the corrosion properties of the fusion zones was investigated. In addition to the heat treatment that the metal alloy is exposed to due to the welding process, the pH values and temperature of the solution environment to which the alloy is exposed also affect the corrosion behavior. [45–49]. It is known that metals exposed to acidic environments and high temperatures have an increased tendency to corrode [50–54]. The fiber laser welded Ti-6Al-4V alloy rods corrosion characteristics have been interpreted by examining 0.9 wt% NaCl solution at pH3 and 5 values and at 25 and 50 ˚C temperatures. Base metal, heat-affected zone and fusion zone microstructures and weight changes after the corrosion test of welded alloys were studied. This study sheds light on the development of fiber laser welding applications of Ti-6Al-4V alloy and reveals the corrosion behavior after welding.

2. Experimental Procedures

Ti-6AI-4V (grade 5) rods with a diameter of 5 mm were used in fiber laser welding applications. The chemical compound of Ti-6Al-4V samples specified in the technical data sheets (TDS) is given in Table 1. Fiber laser welding of the samples was carried out using 300 W LWI V Mobile Flexx II machine using the parameters shown in Table 2 and carried out by a welder in an industrial company. Before the corrosion test, tensile test and Vickers hardness tests were carried out to observe the effect of fiber laser welding on the mechanical properties of the titanium alloy. All samples were used according to ASTM E8M-89b standards to determine the tensile properties. A parallel gauge tensile specimen having a 5 mm diameter and a 25 mm gauge length was prepared with the weld joint at the center of the gauge length. The tensile test performed using universal testing equipment (Model 5982, Instron (100 kN), a screw-driven machine operating at room temperature at a crosshead speed of 2 mm min^{-1}, with a starting strain rate of 0.55×10^{-3} s^{-1}.

Table 1. Chemical composition of Ti-6Al-4V

Element	Weight (%)
Ti	Remaining main part
AI	5.5-6.5
V	3.5-4.5
Fe	0.25
C	0.08
N	0.05
H	0.012
O	0.13

Vickers hardness test was carried out in a TMTECK Micro-hardness tester HV- 1000B using 0.49 kg load (HV0.5) and a dwell time of 15 s. Hardness values were obtained with a total of 9 indentations that recessed at 0.5 mm intervals along the entire specimen surface from the outer surface of the rod specimens as the fusion zone (FZ), towards the center of the specimen the heat affected zone (HAZ), and the base metal zone (BM). After the tensile test, the corrosion test was performed on the cracked surfaces in the welded area. The microstructural and chemical characterization of fractured surfaces after the test was examined with an 80mm^2 X-MAX detector on a JEOL 7001F Field Emission (FE) Scanning Electron Microscope with an EDS attachment. Energy dispersive spectroscopy (EDS) was

used to do a semi-quantitative chemical examination on materials. The process flow chart and schematic representation of laser welding application and corrosion testing are shown in Fig. 1 and 2. In total, 3 groups of samples were prepared and these are the unwelded reference sample and the welded A and B samples, respectively.

Table 2. Fiber laser welding parameters

Parameters	A sample	B sample
Laser Power	73 V	67.5 V
Impact Energy	25.4 J	11.9J
Beam Diameter	900µ	900µ
Pulse Frequency	10 Hz	20Hz
Laser Pulse Width	8.5ms	4.8m

After the fiber laser welding application, the samples were prepared using the metallography method for the microstructural investigations of the welded zones. The preparation process first started by cutting the welded bar samples into small pieces by cutting them in half vertically from the welding areas. The cut sample parts were first molded with the cold bakelite molding method. The molded samples were sanded with abrasives of 180, 320, 600, 800 and 1200, respectively, and then polished with a 1-micron diamond suspension to remove scratches from cutting and sanding and to create a surface that is flawless. After the polishing process, the surfaces were etched and made ready for microscopic examinations. The samples were etched with Kroll's reagent (85 mL H_2O + 10 mL HNO_3 + 5 mL HF) in ASTM E407 solution by keeping them in a magnetic stirrer at 65˚C for 3 minutes. Since Gr 5 Titanium alloys are used as implants in dentistry, the corrosion test environment was prepared based on the changing pH and temperature parameters in the oral environment caused by eating and drinking. It is a well-known phenomenon that acidic and hot beverages corrode tooth enamel and metallic implants than cold ones [55–58]. In addition to temperature and pH changes, it is necessary to examine the effects of internal body environments on these alloys, which are exposed to high heat input due to the welding process.

Previous studies have reported that osteoblasts can be severely damaged by a thermal impulse of 42 ˚C. It has been determined that intraoral temperatures reach 67-77 ˚C during use and hot water/liquid consumption. However, the maximum temperature that living tissue can withstand has been determined as 50 ˚C. In line with similar studies and information, the temperatures chosen to simulate both hot and cool oral environments were 25 and 50 ˚C [59, 60]. To simulate acidic beverage environments, 0.9 wt% NaCl solutions at pH 3 and 5 were prepared using lemon juice.

Table 3. Corrosion test parameters and sample names

Parameters	Samples
pH3 and 25°C	R1, A1 and B1
pH5 and 25°C	R2, A2 and B2
pH3 and 50°	R3, A3 and B3
pH5 and 50°C	R4, A4 and B4

In this way, both more natural ingredients and the most realistic eating and drinking exposure environment were created. The corrosion test was carried out by keeping each sample placed in 50 mL 0.9 wt% NaCl serum at pH3 and 5 and temperatures and 25 and 50 °C in a shaking incubator for 24 hours with stirring. Names and groups of reference and welded samples prepared for corrosion tests are given in Table 3. R samples are control

samples without fiber laser weld jointing. A1, B1, A2, B2, A3, B4, A4 and B4 samples were obtained after the tensile tests of A and B samples welded with the parameters in Table 2. 4 samples were prepared for corrosion testing for both samples A and B.

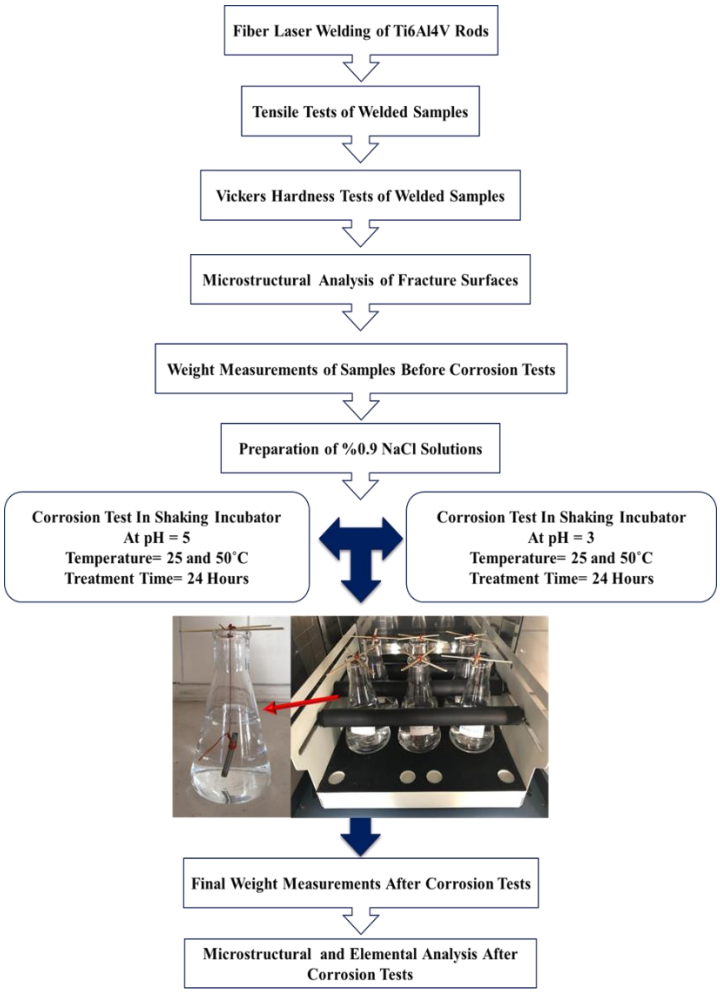

Fig. 1. Process flow chart of the study (İmage shows the samples in NaCl solution and shaking incubator assembly)

The first weights were measured before the samples were placed in the solution. The 0.9 wt% NaCl solution was prepared at pH 3 and 5 and all samples were placed by suspending in the erlenmeyer and shaking incubator as shown in Fig.1. All samples placed in the solution were kept in the shaking incubator according to pH groups for 24 hours at 25° C and 50° C, respectively. After the samples were kept in a shaking incubator for 24 hours, they were removed from erlenmeyer and dried at 27° C in the oven. Finally, after the corrosion test, the final weights of the samples were measured and the test was terminated.

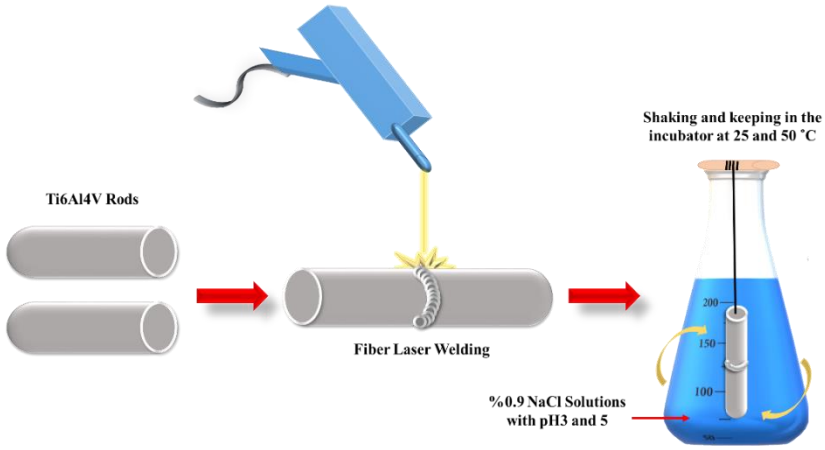

Fig. 2. Schematic representation of laser welding application and corrosion testing

3. Results and Discussion

3.1. Tensile Tests and Vickers Hardness

The images of the samples subjected to the tensile test before and after the test are given in Fig. 3. Since titanium is a highly ductile and durable metal, the non-welded R sample showed a ductile fracture behavior as expected. The fracture surface of the R sample used as a control has a conical structure as shown in Fig. 3. It was observed that the tensile strength of the R sample (957 MPa) matched the values given in the literature [61, 62]. After the tensile test, the A and B specimens were brittlely fractured from their welded parts to be parallel and straight to the rod specimen sections. The heat input used in the welding process of the A sample, which is two times more than that of the B sample, caused the weld depth of the A sample to be greater and the weld seems to be wider. Since the metal has a faster melting and cooling time with high heat input, the weld seam narrows as the heat input increases. While the weld seam thickness of sample A was 9 mm, sample B was 6mm. Insufficient weld depths of the A and B samples caused the joint strength and tensile strength to decrease 9 times compared to the R sample. In addition, the brittle structure resulting from martensitic transformations in the weld area also reduced the tensile strength of the joint areas. This decrease in the tensile strength of the welded parts is an expected situation. Studies [63–65] have shown that this decrease and rupture occurs with a brittle fracture behavior.

As shown in Fig.3, the edges of the outer surfaces of the rods are fusion zones (completely melted) and as it moves inwards from the surface area of the metal, first the HAZ is reached and then the base metal. Fig. 4(b) shows the microhardness distributions in the cross-section of the fusion zone, HAZ and BM zones of the samples. Fig.4(c-d) SEM images show that martensitic α' (dendritic) formations occur in the fusion region. This phase, which is caused by high heat input and rapid cooling in the FZ, increased the hardness of the FZs for A and B samples by 4-23% and 16-31%, respectively, compared to the BM. Higher welding speeds, or less heating input, cause the coarser α′ martensite microstructure to develop within the finer β grains, which increases the hardness values of the B sample in the welding alloy [66]. While the highest hardness value of the fusion zone for sample A was 438 HV0.5, it was calculated as 501 HV0.5 for sample B. The hardness values of the BM were measured as 338 and 341 HV0.5. These values can be considered as standard for Ti-6Al-4V alloy. Omoniyi et al. [62] joined Ti-6Al-4V sheets with 2.6-2.8 kW power values

using laser welding. Vickers hardness measurements showed that the BM was 343 ± 12 HV0.5 and the weld zones were 426 ± 17 HV0.5. Chen et al. [61] showed the BM hardness values of the titanium sheets joined by laser welding using a power of 2.2 kW in the range of 280-300 HV0.5, and the values of the FZ as 372 HV0.5.

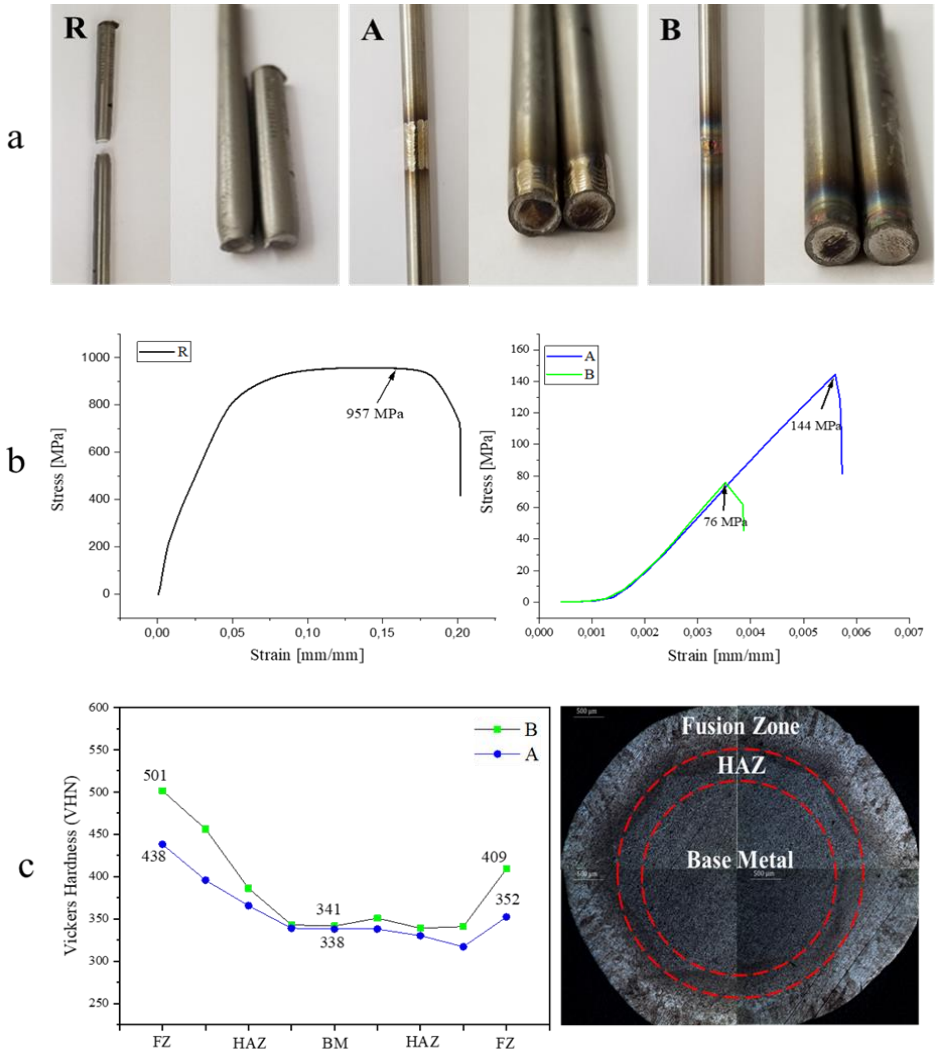

Fig. 3. (a) Non-welded R and fiber laser welded A and B sample images before and after tensile tests, (b) Tensile test result graphs and (c) Vickers Hardness test result graph of reference and fiber laser welded A and B specimens

When the test results are considered, the tensile strengths are decreased and Vickers hardness are increased due to the increase of the laser beam impact energy. This is because, it can be shown that the microstructure of the weld zones of samples as can be seen from Fig.5(c-d), together with the high temperature and rapid cooling used during the welding process, makes the metal structure brittle and hard due to the presence of α'-martensite [67, 68, 68].

3.2. Weight Changes with Temperature and pH

Acicular α′ martensites in the columnar β grains formed in the fusion regions of samples A and B, which were exposed to high heat input during welding, changed the microstructure. As a result of this change, the changes in the fracture fusion surfaces that occurred after the tensile test were observed in the saltwater environment. In this way, the effect of the welding process on the corrosion behavior of the titanium alloy was investigated. Fig.4 shows the weight changes of the reference sample and the welded samples after the corrosion test comparatively. Weight changes at each pH and temperature values are shown in separate graphs. The results show that the weight changes of the fiber laser welded samples differ from each other in varying temperature and pH environments.

As can be clearly seen from Fig.5, the fusion zones of the Ti-6Al-4V alloy had a two-phase α/ and α microstructure. The alloy's tendency to corrosion changed due to this microstructural alteration during laser welding. In the post-weld cooling process, the previous β phase shifts into a stable α phase. The α phase nucleates homogeneously in the previous β phase columnar grains and expands spontaneously up to the grain boundaries. The rates of α-phase nucleation are heavily dependent on the initial laser power temperature and the post-process cooling rates. It is established that the α plate's thickness diminishes with increasing cooling rate. The α phase degradation is an important factor in changing the corrosion properties of Ti-6Al-4V alloys. In addition, the homogeneous allocation of both α and β phases obtained from alloying elements in the structure also plays an important role in corrosion behavior [37]. As presented in Eq. (1), (2), (3), (4), the detailed mechanism of removing the passive layer occurs after immersion in NaCl solution with the formation of novel passive film as a result of the protons' decrease produced during the oxidation of titanium. This mechanism indicates the possible formation of a TiO_2 layer that may have formed on the surface of the samples. The mechanism introduces further metal disintegration and oxide production, with a completely decreased hydrogen state promoting the formation of hydrides in the solution interface layer [69].

$$Ti \rightarrow Ti3+ + 3e- \quad (1)$$

$$Ti + 2H2O \rightarrow TiO2 + 4H+ + 4e- \quad (2)$$

$$H+ + e- \rightarrow H \quad (3)$$

$$Ti3+ + H2O \rightarrow TiO2+ + 2H+ + e- \quad (4)$$

The dissolution of the passive oxide layer after processing the fiber laser welded fractured surfaces in aqueous NaCl solution has been characterized by use of EDS and weight loss analyses. Based on the elemental combination of the EDS results in Table 4, a high variation is seen in the samples' nominal substance after NaCl treatment. Some surface passive layers, such as oxides or carbides, may be the cause of the discrepancy. After 24h of treatment with an aqueous 0.9 wt. % NaCl solution, the highest weight loss observed was 0.0025 g for B4 sample. In the NaCl environment with high temperature and lower hydrogen density, the amount of dissolution on the metal surface increased. The low pH(3) environment caused metal dissolution on the surface of the R1 sample. Some of the dissolved Ti elements accumulated as TiO_2 as seen in Fig.6. It is observed that weight increase occurred in reference samples at 50˚C and pH 5 environments.

This increase is due to the thickening of the oxide layer on the surface with the decrease in the amount of hydrogen, and in addition, the dissolution of more metal and the formation of various oxides and carbides on the surface. Since titanium is a metal with low thermal conductivity, the cooling rate after laser welding is also significantly lower. As the cooling

rate decreases, the transformation rate from the β phase to the α martensite phase decreases and the grain size becomes thicker. It is known that as the phase and grain sizes increase, the corrosion resistance decreases [37]. For this reason, the weight losses on the laser-welded surfaces were discovered to be greater than the reference samples. Similarly, it has been determined that an increase in temperature to 50°C causes an increase in weight loss. The fact that the weight loss is less than that of the B4 sample may be the large size NaCl crystallization seen on the surface of the A3 sample in Fig. 6.

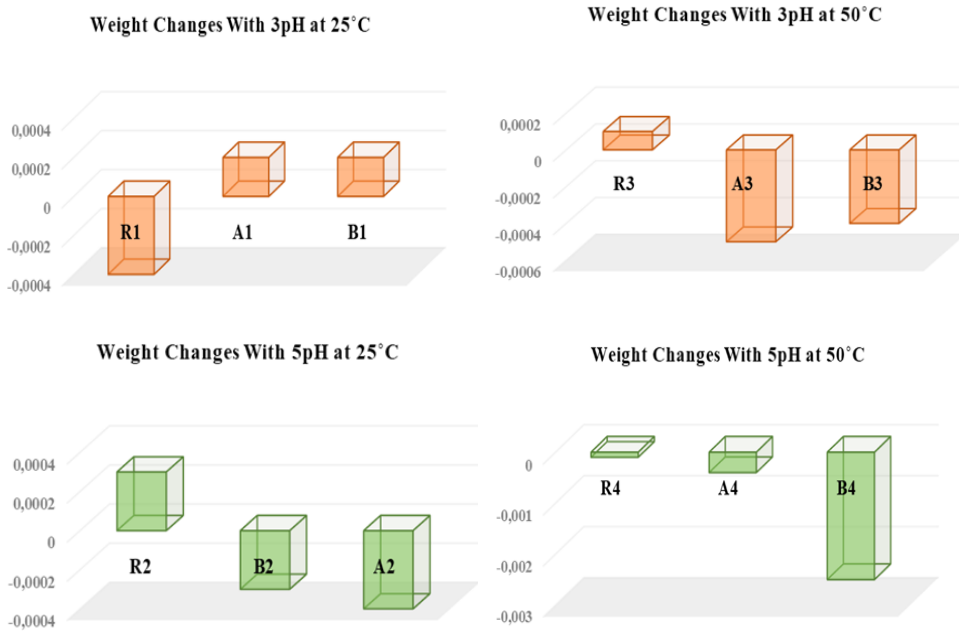

Fig. 4. Weight changes after corrosion tests at different pH and temperature conditions

Table 4. The highest weight differentiated samples EDS element compositions before and after NaCl treatment

Sample	Element	Atomic% Ti-6Al-4V		Weight Change
		Before NaCl Treatment	After NaCl Treatment	
R1	Ti	89,7	77,9	-0,0004
	Al	6	5,6	
	V	4	3,1	
	O	0	6,2	
B4	Ti	82,8	51,5	-0,0025
	Al	5,5	3	
	V	3,4	2,2	
	O	0	4,1	
A3	Ti	81,3	66	-0,0005
	Al	4,9	4,4	
	V	3	2,8	
	O	0	5,7	

It was also seen that the oxygen (O) ratios in Table 4 were in the order of R1>A3>B4 and the weight losses had the reverse order. The increase in the amount of oxygen on the surfaces indicates the amount of the oxide layer formed. Since the oxide layers act as a protector, the weight loss that occurs on the surfaces where the presence of oxide is higher is lower. It has been revealed that the durability to corrosion of the samples exposed to the fiber laser welding process after NaCl interaction decreases and this resistance decreases with the increase in temperature and the pH value of the environment.

3.3. Microstructural Analysis

Before the corrosion test, microstructural characterization of the FZ, HAZ and BM was performed from the metallographic prepared. The microstructure of the BM Ti-6Al-4V consists mainly of white coaxial intergranular β-phase and gray coaxial spherical α-phase, as shown in Fig.5(a) at low and high magnification of SEM image. The intergranular β-phase in the BM is scattered throughout the matrix of the spherical α-phase with various grain sizes. Kroll's reagent's strong oxidizing capability can etch the α phase, so It looks like darker in comparison to the β phase. Therefore, the β phase appears brighter in SEM images [70]. The fiber laser welding process is divided into two stages: heating and cooling, and the microstructure of the Ti-6Al-4V alloy is affected by the cooling rate. During the heating phase, the volume fraction of the β-phase increases and completely converts into the β-phase at 975 °C, and the β-phase remains stable up to 1605 °C. Depending on the cooling rate, the phase transformation ensures that the welded joint takes place from α to β in the heating phase and from β to α/α'' in the cooling phase in the ITAB and fusion zone. When the heat input is low, the cooling rate is faster; when the heat input is large, the cooling rate is slower. When a large amount of heat is applied, the temperature of the fusion zone and the BM rises, and the thermal gradient difference between the fusion zone and the one next to BM reduces, triggering the formation of the transition zone HAZ [21, 63]. The HAZ microstructure seen in Fig.5(b) consisted predominantly of α contains a little quantity of primary α near the weld metal.

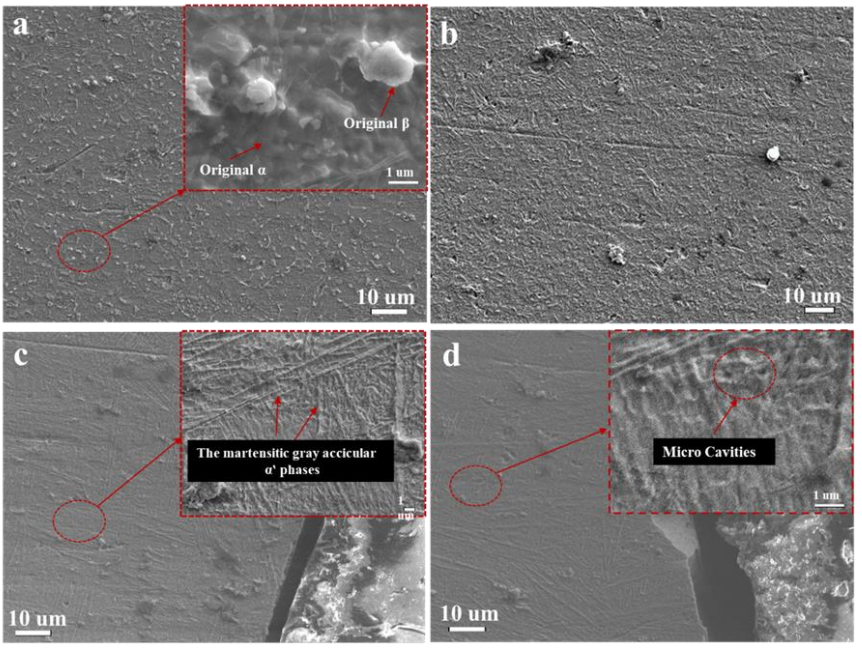

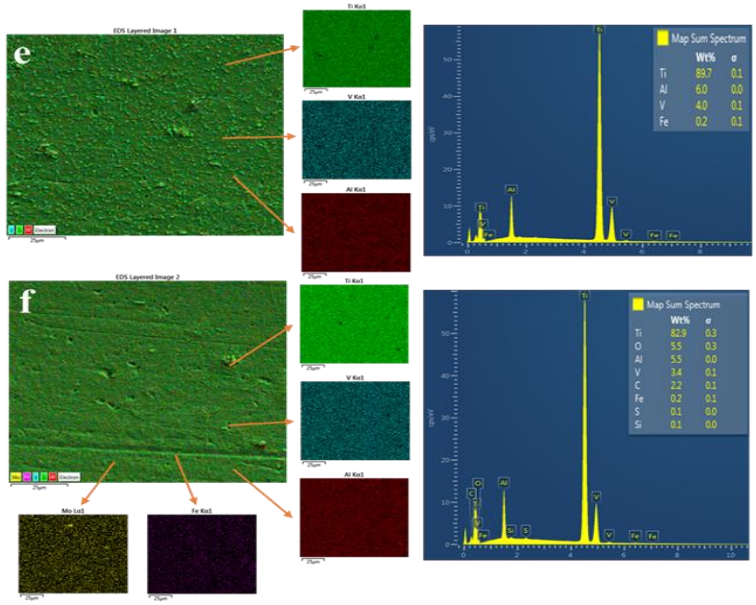

Fig. 5. SEM images of (a) base metals, (b) heat affected zones, (c) A3 sample fusion zone, (d) B4 sample fusion zone and EDS results of (e) base metals, (f) fusion zones before NaCl treatment

As shown in Fig.5(c-d), the microstructure features of the FZ are mostly composed of gray acicular α' martensite, a supersaturated, unstable α phase generated by diffusionless transition of the β phase. The acicular α' martensite microstructure of the fusion region of sample A3 is larger and more homogeneous than the colonies in the microstructure of sample B4. Microstructure investigations showed that the phases in FZ have a coarse martensite microstructure when energy input is increased, as shown in Fig.5(c-d). In addition, it was determined that microcavities due to insufficient melting occurred in the fusion region of the B4 sample, which was welded with lower energy. Fig.5(e-f) EDS mapping results show that the elemental distribution in the fusion region, unlike the BM region, contains 82.9% Ti, 5.5% Al, 5.5% O, 3.4% V and other different elements.

While the ratios of titanium, aluminum and vanadium decreased, the amount of oxygen on the surface increased significantly. This is due to the oxygen absorbed to the surface with temperature and melting during the titanium welding process, which is sensitive to oxygen. The presence of oxygen may also have caused the creation of a passive protective TiOx layer on the titanium alloy surface. Apart from this, it was observed that different elements from the environment and solder metal penetrated the surface at very low rates.

The SEM images given in Fig.6 show that the fractured surface occurs as a typical ductile fracture after the tensile test. The fracture surface is similar to the fracture surface images shown in the literature [71–73] and shows a typical ductile material behavior, consisting of coaxial pits alongside fluctuations and micro-voids, implying that there has been localized plastic deformation that occurred before fracture. After the corrosion test, SEM and EDS analyses were performed on the fractured surfaces of the samples with the highest weight change. Factors such as microstructural and elemental changes and NaCl crystallization that may have caused weight changes were investigated. The elements detected by SEM and EDS spectrum analyses of the R1 fractured surface after NaCl

treatment shown in Fig.5 mainly contain 31% Ti, 28.1% O, 3.8% Al, 1.4% V, 1.7% Na and 0.5% Cl by weight. This high oxygen content implies that corrosion products or an oxide layer are present on the surface. This was verified by the lower than initial % Ti and Al % in the alloy. It can be said that oxides such as Al_2O_3 and TiO_2 are therefore formed on the surface of the R1 sample [74]. Cui et.al. [75] and Qin et.al. [76] proved that TiO_2, Ti_2O_3 and TiO are the main components of passive films formed by titanium and its alloys. When the oxide coating is forming on the surface of the Ti alloy, TiO and Ti_2O_3 are formed first, and this reaction continues and partially turns up to the greatest valence oxide levels (TiO_2). Because the highly concentrated NaCl environment causes an increase in the halide ion (Cl^-) and this ion has an advantageous impact on the corrosion process. This way, it advances the reactions between the metal and the electrolyte. The change in oxide film thickness with NaCl medium can be attributed to the high Cl- concentration accelerating the conversion from Ti_2O_3 and TiO to TiO_2. Therefore, a thicker and less corrosion-resistant oxide film is formed in NaCl solutions. These reactions can be further accelerated by an increase in temperature or a low-pH environment. It can be said that the TiO_2 oxides formed on the surface of the R1 sample occur with the low pH environment and the presence of Cl^- ions. Similarly, Saha et.al. [77] showed that the anti-corrosion ability of the titanium surface due to Cl- ion attack increased after the production of the nano porous oxide layer. In addition, they stated that the annealed Ti6Al4V sample showed a slightly higher Icorr value than the anodized Ti6Al4V sample, and the corrosion inhibition ability decreased slightly after annealing. It is known that the microstructure obtained by melting at high temperature and then cooling to room temperature reduces the resistance against corrosion and the fiber laser welding process also created this effect. As shown in Fig.6, the decrease in the main alloy element ratios on the surfaces of the laser welded A3 and B4 samples is higher than that of the R1 sample, and the formation of corrosion products such as oxides and salt crystals on the surfaces is due to the reasons mentioned above.

Fig.7 EDS mapping and spectral analyses showed that after NaCl treatment, high levels of C and O elements appeared in the BM and FZ, and similarly Na and Cl elements were present on the surfaces. It is thought that C, O, Fe, Ca, Mg and Si elements, which exist on the surfaces apart from the main alloying elements, adhere to the surface from the external environment during the welding process. The presence of especially high levels of oxygen and carbon indicates that various oxides and carbides may have formed on the surface. C and O are more present at the boundaries connecting the HAZ region to the fusion region, as seen in Fig. 7 EDS-line results.

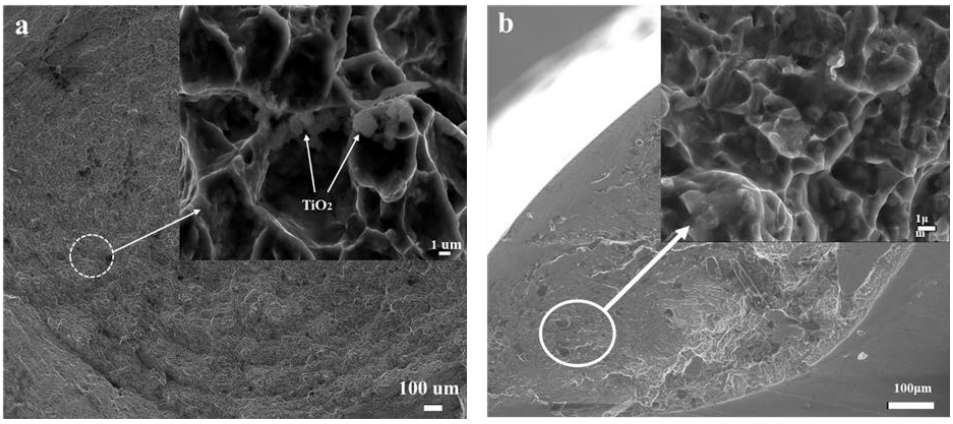

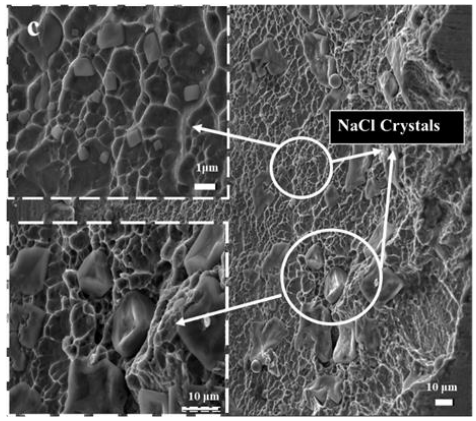

Fig. 6SEM images of (a) R1, (b) B4 and (c) A3 fracture surfaces after corrosion test

Since these regions are more protruding and porous, it was expected that oxygen and corrosion products adhere to the surface more. It is assumed that while some of the Na and Cl elements accumulated on the surface dissolve as salt crystals, the other part forms various nanostructures on the surface. Various studies have proven that Na^+ and Cl^- ions serve a significant influence in the formation of nanostructures and oxides. Yang et.al. [78] were produced hematite (α-Fe_2O_3) nanoplates with using NaCl, which is an N-type semiconductor. Due to the positive charge of the (α-Fe_2O_3) nanoplates, Due to hydrogen bonding between the positive and negative charge, they were coated with a layer of Cl^- ions when redistributed in a NaCl solution. The accumulation of Na^+ ions resulted in the formation of NaCl crystals and thus the self-assembly of the nanoplates. Because of its outstanding resistance to corrosion and diverse commercial and industrial uses in domains such as catalysts, magnetic devices, pigments, gas sensors, and rechargeable, it is a stable and valuable material. They are used in lithium-ion batteries in addition to other biological and medicinal disciplines. Shi et al. [79] synthesize monolayer WS2 crystals on SiO_2/Si substrate which is one typical example of the semiconducting transition-metal dichalcogenides (TMDCs) materials in one semi-sealed quartz tube, by utilizing NaCl as a growth stimulant. They also stated that the WS2 crystals' quantity and size have increased astoundingly throughout the time NaCl is introduced. Liu et al. (2014) [80] investigated in the selective photocatalytic destruction of CIP, a novel surface molecular imprinted NaCl/TiO_2 photocatalyst was developed. Chlorine was utilized in the solid-state approach to dope TiO_2. Among the chlorides, NaCl/TiO_2 nanomaterials had the highest photocatalytic activity of K^+, Na^+, Mg_2^+, $NH4^+$, Zn_2^+ and Ba_2^+. Shu et.al. (2020) [81] used a NaCl-based solid-solution technique to create porous metal oxides containing finely distributed noble metal NPs in a one-pot process. The well-dispersion of metal chlorides on NaCl, i.e. the mechanochemical production of MClx-NaCl solid solution, was discovered to be a critical step in controlling the porosity of metal oxides and the dispersion of noble metal species. In this approach, a number of porous metal oxides and related catalysts (FexOy, Cr_2O_3, Co_3O_4, Pd-FexOy, Pt-Cr_2O_3, and Rh-Co_3O_4) have been developed and successfully be prepared. In summary, Na^+ and Cl^- ions positively affect the synthesis and production of metallic nanoparticles, oxides and catalysts. Studies have also shown that Cl ions attack metal ions and create new structures. The 0.9 wt% NaCl solution was the cause of the reduction of the main metal alloy elements seen on the surfaces after the corrosion test and the formation of oxides of oxygen, carbon and other elements on the surface. These formations were triggered more by increasing temperature and decreasing pH. The increase in NaCl crystals and oxide layer formation also increases the resistance of the

metal against corrosion. It was determined that the weight change results given in Fig.4 were directly proportional to the SEM and EDS results. Because the weight losses in the A3 and R1 samples, where the salt crystals and TiO_2 oxides are more, were much lower than in the B4 sample. This proves that corrosion-induced wear on the metal surface or ion distribution is less. SEM and EDS mapping and spectrum results of the BM and FZ of sample A3 presented in Fig.6 show that high rates of salt crystals are formed on the surfaces. Na and Cl elements, present at the rates of 1.1% and 0.5% in the BM, increased to 16.5% and 11.5% in the fusion region. The reason for this can be shown that the martensite structure in the fusion region has a lower resistance to corrosion and that Cl- ions and oxygen are more absorbed into the surface. The EDS-line results given in Fig.6(c) also clearly showed that the presence of Na and Cl elements increased sharply from the BM to the fusion zone. In the B4 sample, on the other hand, it was determined from the EDS-line analysis that the NaCl ratios in the BM and FZ were very low and at the same ratios. NaCl salts crystallized in the A3 fusion region are {1 0 0} and {1 1 1} hopper-shaped forms. In Ref. [50, 82, 83] studies, they claimed that hopper cubes and tiny vicinal faces of the octahedron are created. The top (1 1 1) face of a NaCl crystal nucleated with a triad axis nearly parallel to the glass substrate will also develop approximately hopper-shaped.

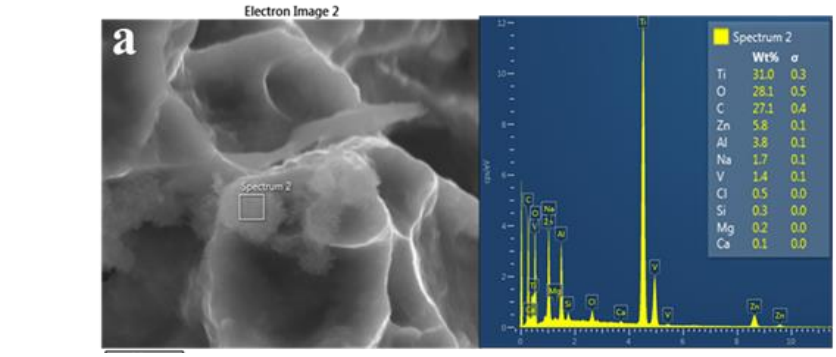

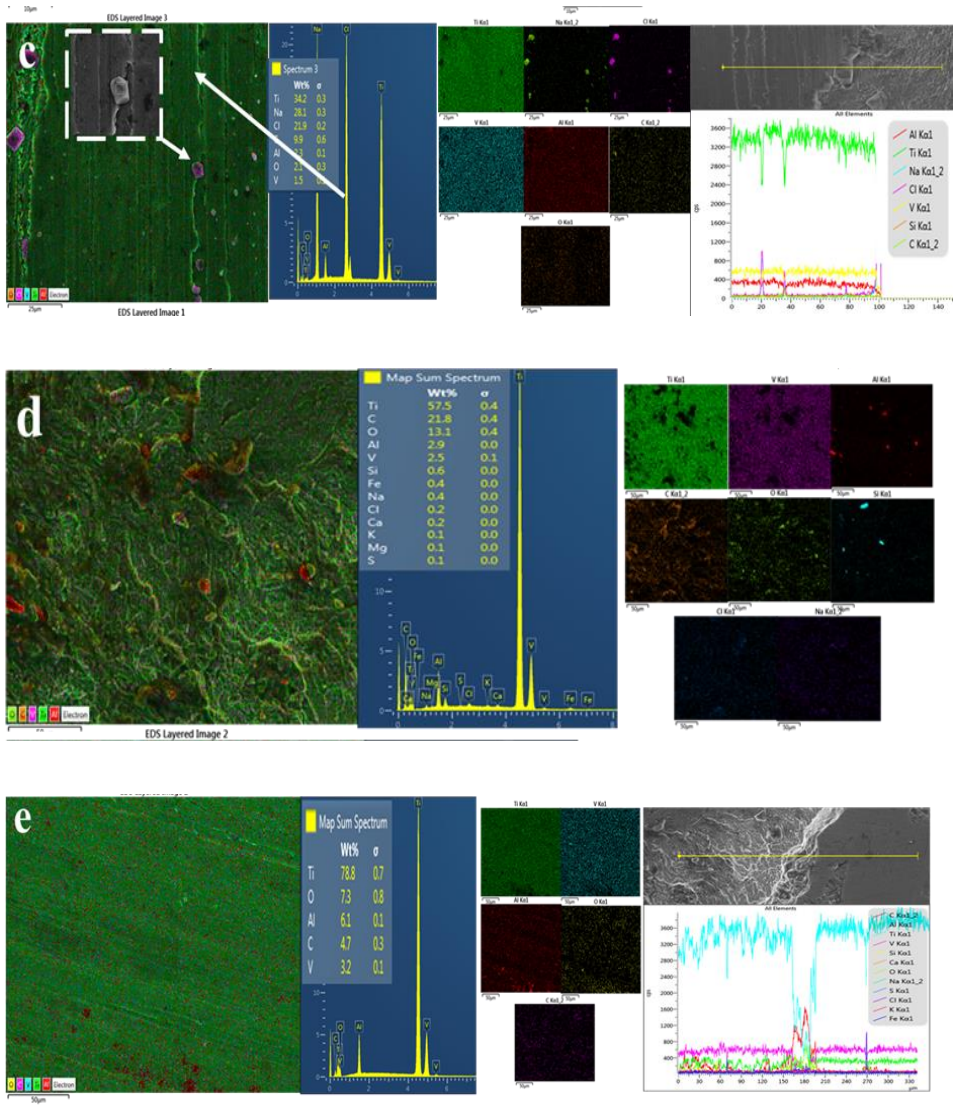

Fig. 7. EDS distribution of the elements on (a) R sample, (b) fusion zone of A3, (c) base metal of A3, and (d) fusion zone of B4, (e) base metal of B4

It was determined that the salt crystals and TiO2 on the surface of the fiber laser welded A3 sample, together with the combination of low pH and NaCl environment, allowed it to grow critically more than the B4 sample. Apart from this, according to the Vickers hardness values in Fig.3(b), the martensitic transformations of the FZ region of the A3 sample combined with higher welding energy, causing higher hardness than BM, are more sensitive to corrosion products than the other welded samples. created. The sizes of these formed crystals were calculated using the Image J program on SEM images. The crystal sizes range from 2-10 μm and they average 8 μm in size.

5. Conclusions

Ti-6Al-4V alloy rods, which are of great importance in biomedical and industrial applications, were joined by fiber laser welding technology. Tensile and microhardness mechanical tests were carried out after the welding process. Among the welded samples, the highest strength was obtained in sample A with 134 MPa. The hardness tests performed on the surfaces after the welding process showed that the a' martensitic phase transformation in the fusion zone increased the hardness values on average 1.5 times. For the purpose of determining the corrosion behavior of the fiber laser welded Ti-6Al-4V (Gr5) rod alloys fractured surfaces after the tensile test by creating a naturally corrosive and hot environment. The samples were exposed to pH3-5, 25-50°C temperatures and 0.9 wt% NaCl environment for 24 hours in a shaking incubator. According to the weight change measurements made before and after the corrosion test, the highest weight loss occurred in the B4 sample with 0.0025 g. The microstructure changes and formations on the fractured surfaces before and after NaCl treatment were compared with SEM and EDS analyses. The formation of gray acicular a' martensitic phases was observed in the fusion and heat-affected zones. It has been shown that the fusion zones tend to react with more oxygen than the BM, leading to TiO_2 oxide formations and NaCl crystallizations. It was determined that the FZ regions, whose hardness values increased after welding, had a higher tendency to undergo corrosion. NaCl crystals and oxide layer, which formed on the A3 sample have significant and larger sizes compared to the B4 sample. These layers increased the corrosion resistance of this sample and provided a very low weight loss of 0.0005. The damaged area in Ti-Al-4V implants was simulated with the fractured surface created by the tensile test after joining with fiber laser welding. It was understood that due to the martensitic microstructure changes and the rough structure that occurred after the tensile test, the fusion regions were more prone to corrosion in high-temperature and low-pH environments. Apart from these, it has been proven that NaCl crystallization conditions are met and that small-size (8um) crystals can be obtained. In this way, a method was introduced to obtain hopper-shaped NaCl that can be used to synthesize various catalysts, oxides and nanostructures.

Acknowledgment

All studies were conducted at Ondokuzmayıs University, Faculty of Engineering, Metallurgical and Materials Engineering Laboratory.

References

[1] Anuwar M, Jayaganthan R, Tewari VK, Arivazhagan N. A study on the hot corrosion behavior of Ti-6Al-4V alloy. Materials Letters 2007; 61(7): 1483-8 https://doi.org/10.1016/j.matlet.2006.07.058

[2] Ciszak C, Popa I, Brossard J-M, Monceau D, Chevalier S. NaCl induced corrosion of Ti-6Al-4V alloy at high temperature. Corrosion Science 2016; 110: 91-104 https://doi.org/10.1016/j.corsci.2016.04.016

[3] Krząkała A, Służalska K, Dercz G, et al. Characterization of bioactive films on Ti-6Al-4V alloy. Electrochimica Acta 2013; 104: 425-38 https://doi.org/10.1016/j.electacta.2012.12.081

[4] López MF, Gutiérrez A, Jiménez JA. In vitro corrosion behaviour of titanium alloys without vanadium. Electrochimica Acta 2002; 47(9): 1359-64. https://doi.org/10.1016/S0013-4686(01)00860-X

[5] Rodrigues DC, Valderrama P, Wilson TG, et al. Titanium Corrosion Mechanisms in the Oral Environment: A Retrieval Study. Materials (Basel) 2013; 6(11): 5258-74. https://doi.org/10.3390/ma6115258

[6] Yao Z, Marck M. NaCl-induced hot corrosion of a titanium aluminide alloy. Materials Science and Engineering: A 1995; 192-193(10): 994-1000. https://doi.org/10.1016/0921-5093(95)03345-9
[7] BALOYI NM, Popoola API, Pityana SL. Microstructure, hardness and corrosion properties of laser processed Ti6Al4V-based composites. Transactions of Nonferrous Metals Society of China 2015; 25(9): 2912-23. https://doi.org/10.1016/S1003-6326(15)63917-6
[8] Gil FJ, Delgado L, Espinar E, Llamas JM. Corrosion and corrosion-fatigue behavior of cp-Ti and Ti-6Al-4V laser-marked biomaterials. J Mater Sci Mater Med 2012; 23(4): 885-90. https://doi.org/10.1007/s10856-012-4572-z
[9] Khan MA, Williams RL, Williams DF. The corrosion behaviour of Ti-6Al-4V, Ti-6Al-7Nb and Ti-13Nb-13Zr in protein solutions. Biomaterials 1999; 20(7): 631-7. https://doi.org/10.1016/S0142-9612(98)00217-8
[10] Lin X-z, Zhu M-h, Cai Z-b, Dou B-j, Cui X-j. Torsional fretting corrosion behaviours of Ti6Al4V alloys in Hank's simulated body fluid. Corrosion Engineering, Science and Technology 2019; 54(4): 298-309. https://doi.org/10.1080/1478422X.2019.1589675
[11] Singh R, Martin M, Dahotre NB. Influence of laser surface modification on corrosion behavior of stainless steel 316L and Ti-6Al-4V in simulated biofluid. Surface Engineering 2013; 21(4): 297-306. https://doi.org/10.1179/174329405X55320
[12] Xu Y, Lu Y, Sundberg KL, Liang J, Sisson RD. Effect of Annealing Treatments on the Microstructure, Mechanical Properties and Corrosion Behavior of Direct Metal Laser Sintered Ti-6Al-4V. J. of Materi Eng and Perform 2017; 26(6): 2572-82. https://doi.org/10.1007/s11665-017-2710-y
[13] Zaveri N, McEwen GD, Karpagavalli R, Zhou A. Biocorrosion studies of TiO2 nanoparticle-coated Ti-6Al-4V implant in simulated biofluids. J Nanopart Res 2010; 12(5): 1609-23. https://doi.org/10.1007/s11051-009-9699-6
[14] Jáquez-Muñoz JM, Gaona-Tiburcio C, Cabral-Miramontes J, et al. Electrochemical Noise Analysis of the Corrosion of Titanium Alloys in NaCl and H2SO4 Solutions. Metals 2021; 11(1): 105. https://doi.org/10.3390/met11010105
[15] Ertek Emre H. The corrosion behaviour of as-welded and post-weld heat treated Ti6Al4V alloy in simulated body fluid. Materials Letters 2019; 254(3): 162-6. https://doi.org/10.1016/j.matlet.2019.07.056
[16] Garcia-Ramirez MJ, Lopez-Sesenes R, Rosales-Cadena I, Gonzalez-Rodriguez JG. Corrosion behaviour of Ti-Ni-Al alloys in a simulated human body solution. Journal of Materials Research and Technology 2018; 7(3): 223-30. https://doi.org/10.1016/j.jmrt.2017.07.003
[17] Karimzadeh F, Heidarbeigy M, Saatchi A. Effect of heat treatment on corrosion behavior of Ti-6Al-4V alloy weldments. Journal of Materials Processing Technology 2008; 206(1-3): 388-94. https://doi.org/10.1016/j.jmatprotec.2007.12.065
[18] Manam NS, Harun WSW, Shri DNA, et al. Study of corrosion in biocompatible metals for implants: A review. Journal of Alloys and Compounds 2017; 701(3): 698-715. https://doi.org/10.1016/j.jallcom.2017.01.196
[19] Yang X, Dong X, Li W, Feng W, Xu Y. Effect of solution and aging treatments on corrosion performance of laser solid formed Ti-6Al-4V alloy in a 3.5 wt. % NaCl solution. Journal of Materials Research and Technology 2020; 9(2): 1559-68. https://doi.org/10.1016/j.jmrt.2019.11.082
[20] Zavanelli RA, Guilherme AS, Pessanha-Henriques GE, Arruda Nóbilo MA de, Mesquita MF. Corrosion-fatigue of laser-repaired commercially pure titanium and Ti-6Al-4V alloy under different test environments. J Oral Rehabil 2004; 31(10): 1029-34. https://doi.org/10.1111/j.1365-2842.2004.01336.x
[21] Nabhani M, Shoja Razavi R, Barekat M. Corrosion study of laser cladded Ti-6Al-4V alloy in different corrosive environments. Engineering Failure Analysis 2019; 97: 234-41. https://doi.org/10.1016/j.engfailanal.2019.01.023

[22] 2022 Medical Technologies Congress (TIPTEKNO). IEEE; 2022.
[23] Zhou S, Zhang J, Wang J, Yang G, Wu K, Qin L. Effect of Oxygen Levels in Tent Shielding Atmosphere on Microstructural and Mechanical Properties of Ti-6Al-4V Fabricated by Wire Arc Additive Manufacturing. J. of Materi Eng and Perform 2022; 31(7): 5269-78. https://doi.org/10.1007/s11665-022-06684-w
[24] Yang Z, Li J, Zhang B, Li J. Microstructures and mechanical properties of a titanium alloy thick plate joint after electron beam welding plus solution-aging. Journal of Materials Research and Technology 2022; 19(5-8): 913-22. https://doi.org/10.1016/j.jmrt.2022.05.091
[25] Raut N, Yakkundi V, Sunnapwar V, Medhi T, Jain VKS. A specific analytical study of friction stir welded Ti-6Al-4V grade 5 alloy: Stir zone microstructure and mechanical properties. Journal of Manufacturing Processes 2022; 76(1): 611-23. https://doi.org/10.1016/j.jmapro.2022.02.036
[26] Irmak E, Ugurlu B, Incesu A. Investigation of Tribocorrosion Properties of Titanium Implant used in Orthopedics. In: Investigation of Tribocorrosion Properties of Titanium Implant used in Orthopedics; 2022. IEEE; 1-4. https://doi.org/10.1109/TIPTEKNO56568.2022.9960164
[27] Li C, Muneharua K, Takao S, Kouji H. Fiber laser-GMA hybrid welding of commercially pure titanium. Materials & Design 2009; 30(1): 109-14. https://doi.org/10.1016/j.matdes.2008.04.043
[28] Kuryntsev SV, Morushkin AE, Gilmutdinov AK. Fiber laser welding of austenitic steel and commercially pure copper butt joint. Optics and Lasers in Engineering 2017; 90(9): 101-9. https://doi.org/10.1016/j.optlaseng.2016.10.008
[29] Miranda RM, Assunção E, Silva RJC, Oliveira JP, Quintino L. Fiber laser welding of NiTi to Ti-6Al-4V. Int J Adv Manuf Technol 2015; 81(9-12): 1533-8. https://doi.org/10.1007/s00170-015-7307-8
[30] Quintino L, Costa A, Miranda R, Yapp D, Kumar V, Kong CJ. Welding with high power fiber lasers - A preliminary study. Materials & Design 2007; 28(4): 1231-7. https://doi.org/10.1016/j.matdes.2006.01.009
[31] Hafez KM, Katayama S. Fiber laser weldin g of AISI 304 stainless steel plates. Quarterly Journal of The Japan Welding Society 2009; 27(2): 69s-73s. https://doi.org/10.2207/qjjws.27.69s
[32] Lai R, Cai Y, Wu Y, Li F, Hua X. Influence of absorbed nitrogen on microstructure and corrosion resistance of 2205 duplex stainless steel joint processed by fiber laser welding. Journal of Materials Processing Technology 2016; 231: 397-405. https://doi.org/10.1016/j.jmatprotec.2016.01.016
[33] Miranda R, Costa A, Quintino L, Yapp D, Iordachescu D. Characterization of fiber laser welds in X100 pipeline steel. Materials & Design 2009; 30(7): 2701-7. https://doi.org/10.1016/j.matdes.2008.09.042
[34] Pekkarinen J, Kujanpää V. The effects of laser welding parameters on the microstructure of ferritic and duplex stainless steels welds. Physics Procedia 2010; 5: 517-23. https://doi.org/10.1016/j.phpro.2010.08.175
[35] Zhang L, Lu JZ, Luo KY, et al. Residual stress, micro-hardness and tensile properties of ANSI 304 stainless steel thick sheet by fiber laser welding. Materials Science and Engineering: A 2013; 561: 136-44. https://doi.org/10.1016/j.msea.2012.11.001
[36] Vikas KSR, Rahul, Ramana VSNV, Reddy GM, Rao KS. Influence of heat treatments on corrosion behavior of Ti64 friction welds. Chemical Data Collections 2022; 42(24): 100940. https://doi.org/10.1016/j.cdc.2022.100940
[37] Pazhanivel B, Sathiya P, Sozhan G. Ultra-fine bimodal (α + β) microstructure induced mechanical strength and corrosion resistance of Ti-6Al-4V alloy produced via laser powder bed fusion process. Optics & Laser Technology 2020; 125(6): 106017. https://doi.org/10.1016/j.optlastec.2019.106017

[38] Mahlobo MGR, Chikosha L, Olubambi PA. Study of the corrosion properties of powder rolled Ti-6Al-4V alloy applied in the biomedical implants. Journal of Materials Research and Technology 2022; 18(4): 3631-9. https://doi.org/10.1016/j.jmrt.2022.04.004
[39] Cui Y-W, Chen L-Y, Qin P, et al. Metastable pitting corrosion behavior of laser powder bed fusion produced Ti-6Al-4V in Hank's solution. Corrosion Science 2022; 203: 110333. https://doi.org/10.1016/j.corsci.2022.110333
[40] Lim B-S, Cho H-R, Choe H-C. Corrosion behaviors of macro/micro/nano-scale surface modification on Ti-6Al-4V alloy for bio-implant. Thin Solid Films 2022; 754: 139314. https://doi.org/10.1016/j.tsf.2022.139314
[41] Lebea L, Ngwangwa HM, Desai DA, Nemavhola F. Corrosion Resistance of 3D-Printed Titanium Alloy Ti64-ELI Parts for Dental Application. Appl Bionics Biomech 2022; 2022: 1804417. https://doi.org/10.1155/2022/1804417
[42] Metalnikov P, Ben-Hamu G, Eliezer D. Corrosion behavior of AM-Ti-6Al-4V: A comparison between EBM and SLM. Prog Addit Manuf 2022; 7(3): 509-20. https://doi.org/10.1007/s40964-022-00293-8
[43] Qiao Q, Tam LM, Cristino VAM, Kwok CT. Surface hardness and corrosion behavior of laser surface-alloyed Ti6Al4V with copper. Surface and Coatings Technology 2022; 444(22): 128663. https://doi.org/10.1016/j.surfcoat.2022.128663
[44] Rahmouni K, Besnard A, Oulmi K, et al. In vitro corrosion response of CoCrMo and Ti-6Al-4V orthopedic implants with Zr columnar thin films. Surface and Coatings Technology 2022; 436: 128310. https://doi.org/10.1016/j.surfcoat.2022.128310
[45] Assis Ferreira N de, Senna PM, do Lago DCB, Senna LF de, Sampaio-Filho HR. Influence of stress corrosion on the mechanical properties of laser-welded titanium. J Prosthet Dent 2016; 115(3): 356-62. https://doi.org/10.1016/j.prosdent.2015.09.002
[46] Le Guéhennec L, Soueidan A, Layrolle P, Amouriq Y. Surface treatments of titanium dental implants for rapid osseointegration. Dent Mater 2007; 23(7): 844-54. https://doi.org/10.1016/j.dental.2006.06.025
[47] Mohammed MT, Khan ZA, Siddiquee AN. Surface Modifications of Titanium Materials for developing Corrosion Behavior in Human Body Environment: A Review. Procedia Materials Science 2014; 6: 1610-8. https://doi.org/10.1016/j.mspro.2014.07.144
[48] Pazos L, Corengia P, Svoboda H. Effect of surface treatments on the fatigue life of titanium for biomedical applications. J Mech Behav Biomed Mater 2010; 3(6): 416-24. https://doi.org/10.1016/j.jmbbm.2010.03.006
[49] Vasilescu E, Drob P, Raducanu D, et al. Effect of thermo-mechanical processing on the corrosion resistance of Ti6Al4V alloys in biofluids. Corrosion Science 2009; 51(12): 2885-96. https://doi.org/10.1016/j.corsci.2009.08.014
[50] Aquilano D, Pastero L, Bruno M, Rubbo M. {100} and {111} forms of the NaCl crystals coexisting in growth from pure aqueous solution. Journal of Crystal Growth 2009; 311(2): 399-403. https://doi.org/10.1016/j.jcrysgro.2008.11.006
[51] Elagli K, Traisnel M, Hildebrand HF. Electrochemical behaviour of titanium and dental alloys in artificial saliva. Electrochimica Acta 1993; 38(13): 1769-74. https://doi.org/10.1016/0013-4686(93)85075-A
[52] Fojt J, Joska L, Málek J. Corrosion behaviour of porous Ti-39Nb alloy for biomedical applications. Corrosion Science 2013; 71: 78-83. https://doi.org/10.1016/j.corsci.2013.03.007
[53] Souza JCM, Barbosa SL, Ariza E, Celis J-P, Rocha LA. Simultaneous degradation by corrosion and wear of titanium in artificial saliva containing fluorides. Wear 2012; 292-293(9): 82-8. https://doi.org/10.1016/j.wear.2012.05.030
[54] Vieira AC, Ribeiro AR, Rocha LA, Celis JP. Influence of pH a nd corrosion inhibitors on the tribocorrosion of titanium in artificial saliva. Wear 2006; 261(9): 994-1001. https://doi.org/10.1016/j.wear.2006.03.031

[55] Arakelyan M, Spagnuolo G, Iaculli F, et al. Minimization of Adverse Effects Associated with Dental Alloys. Materials (Basel) 2022; 15(21. https://doi.org/10.3390/ma15217476
[56] Mohammed NB, Daily ZA, Alsharbaty MH, et al. Effect of PMMA sealing treatment on the corrosion behavior of plasma electrolytic oxidized titanium dental implants in fluoride-containing saliva solution. Mater. Res. Express 2022; 9(12): 125401. https://doi.org/10.1088/2053-1591/aca7b5
[57] Nagay BE, Cordeiro JM, Barao VAR. Insight Into Corrosion of Dental Implants: From Biochemical Mechanisms to Designing Corrosion-Resistant Materials. Curr Oral Health Rep 2022; 9(2): 7-21. https://doi.org/10.1007/s40496-022-00306-z
[58] Paolone G, Mandurino M, Pavan F, Mazzitelli C, Cantatore G. Novel Dental Restorative Solutions for Natural Teeth and Implants. Bioengineering (Basel) 2022; 9(12). https://doi.org/10.3390/bioengineering9120772
[59] Arakji H, Osman E, Aboelsaad N, Shokry M. Evaluation of implant site preparation with piezosurgery versus conventional drills in terms of operation time, implant stability and bone density (randomized controlled clinical trial- split mouth design). BMC Oral Health 2022; 22(1): 567. https://doi.org/10.1186/s12903-022-02613-4
[60] Thadathil Varghese J, Babaei B, Farrar P, Prentice L, Prusty BG. Influence of thermal and thermomechanical stimuli on a molar tooth treated with resin-based restorative dental composites. Dent Mater 2022; 38(5): 811-23. https://doi.org/10.1016/j.dental.2022.04.010
[61] Chen Z, Wang B, Duan B. Mechanical Properties and Microstructure of a High-Power Laser-Welded Ti6Al4V Titanium Alloy. J. of Materi Eng and Perform 2020; 29(4): 2296-304. https://doi.org/10.1007/s11665-020-04737-6
[62] Omoniyi P, Mahamood R, Arthur N, et al. Laser Butt Welding of Thin Ti6Al4V Sheets: Effects of Welding Parameters. J. Compos. Sci. 2021; 5(9): 246. https://doi.org/10.3390/jcs5090246
[63] Ertek Emre H, Arslan Ş. Effect of laser welding on microstructure and mechanical properties of biomedical Ti6Al4V. Appl. Phys. A 2019; 125(11): 1071. https://doi.org/10.1007/s00339-019-3045-3
[64] Kumar P, Sinha AN. Effect of heat input in pulsed Nd: YAG laser welding of titanium alloy (Ti6Al4V) on microstructure and mechanical properties. Weld World 2019; 63(3): 673-89. https://doi.org/10.1007/s40194-018-00694-w
[65] Sepe R, Franchitti S, Borrelli R, Di Caprio F, Armentani E, Caputo F. Correlation between real geometry and tensile mechanical behaviour for Ti6Al4V electron beam melted thin specimens. Theoretical and Applied Fracture Mechanics 2020; 107(3): 102519. https://doi.org/10.1016/j.tafmec.2020.102519
[66] Rominiyi AL, Mashinini PM. Continuous wave laser welding of Ti6Al4V alloy joints: Microstructure and mechanical properties. Materials Letters 2023; 336: 133934. https://doi.org/10.1016/j.matlet.2023.133934
[67] Ohkubo C, Watanabe I, Ford JP, Nakajima H, Hosoi T, Okabe T. The machinability of cast titanium and Ti-6Al-4V. Biomaterials 2000; 21(4): 421-8. https://doi.org/10.1016/S0142-9612(99)00206-9
[68] Meyer U, Bühner M, Büchter A, Kruse-Lösler B, Stamm T, Wiesmann HP. Fast element mapping of titanium wear around implants of different surface structures. Clin Oral Implants Res 2006; 17(2): 206-11. https://doi.org/10.1111/j.1600-0501.2005.01184.x
[69] Pazhanivel B, Sathiya P, Muthuraman K, Sozhan G. Influence of NaCl environment on stress corrosion cracking of additive manufactured Ti-6Al-4V alloy. Engineering Failure Analysis 2021; 127: 105515. https://doi.org/10.1016/j.engfailanal.2021.105515
[70] Shahsavari M, Imani A, Schaller RF, Asselin E. Corrosion evaluation of Ti-6Al-4V manufactured by electron beam melting in Ringer's physiological solution: An in vitro

study of the passive film. J Appl Electrochem 2022; 52(6): 1003-19. https://doi.org/10.1007/s10800-022-01683-0
[71] Fernandes MF, Oliveira Velloso VMd, Cornelis Voorwald HJ. Investigation of the damage and fracture of Ti-6Al-4V titanium alloy under dwell-fatigue loadings. Procedia Structural Integrity 2022; 35: 141-9. https://doi.org/10.1016/j.prostr.2021.12.058
[72] Gao F, Sun Z, Yang S, Jiang P, Liao Z. Stress corrosion characteristics of electron beam welded titanium alloys joints in NaCl solution. Materials Characterization 2022; 192(1): 112126. https://doi.org/10.1016/j.matchar.2022.112126
[73] Wang Y, Zhao H, Ma H, Zhang Y. The effect of thickness on fracture characteristics of TC4 titanium alloy sheets. Archiv.Civ.Mech.Eng 2022; 22(4): 129. https://doi.org/10.1007/s43452-022-00473-x
[74] Abdo HS, Sherif E-SM, El-Serehy HA. Manufacturing of Ti-6%Al and Ti-6%Al-4%V Alloys and Their Corrosion in Sodium Chloride Solutions. Crystals 2020; 10(3): 181. https://doi.org/10.3390/cryst10030181
[75] Cui Y-W, Chen L-Y, Chu Y-H, et al. Metastable pitting corrosion behavior and characteristics of passive film of laser powder bed fusion produced Ti-6Al-4V in NaCl solutions with different concentrations. Corrosion Science 2023; 215: 111017. https://doi.org/10.1016/j.corsci.2023.111017
[76] Qin P, Chen LY, Liu YJ, et al. Corrosion and passivation behavior of laser powder bed fusion produced Ti-6Al-4V in static/dynamic NaCl solutions with different concentrations. Corrosion Science 2021; 191: 109728. https://doi.org/10.1016/j.corsci.2021.109728
[77] Saha SK, Park YJ, Cho SO. Fabrication of highly ordered nanoporous oxide layer on Ti6Al4V surfaces for improved corrosion resistance property. Journal of Molecular Structure 2021; 1223: 129244. https://doi.org/10.1016/j.molstruc.2020.129244
[78] Yang P, Wang D, Zhao J, Shi R. Facile synthesis of hematite nanoplates and their self-assembly generated by domain growth of NaCl. Materials Research Bulletin 2015; 65(13): 36-41. https://doi.org/10.1016/j.materresbull.2015.01.002
[79] Shi B, Zhou D, Qiu R, et al. High-efficiency synthesis of large-area monolayer WS2 crystals on SiO2/Si substrate via NaCl-assisted atmospheric pressure chemical vapor deposition. Applied Surface Science 2020; 533: 147479. https://doi.org/10.1016/j.apsusc.2020.147479
[80] Liu X, Lv P, Yao G, et al. Selective degradation of ciprofloxacin with modified NaCl/TiO2 photocatalyst by surface molecular imprinted technology. Colloids and Surfaces A: Physicochemical and Engineering Aspects 2014; 441(208): 420-6. https://doi.org/10.1016/j.colsurfa.2013.10.005
[81] Shu Y, Chen H, Chen N, et al. A Principle for Highly Active Metal Oxide Catalysts via NaCl-Based Solid Solution. Chem 2020; 6(7): 1723-41. https://doi.org/10.1016/j.chempr.2020.04.003
[82] Madsen RSK, Motuzas J, Vaughan J, Julbe A, Diniz da Costa JC. Fine control of NaCl crystal size and particle size in percrystallisation by tuning the morphology of carbonised sucrose membranes. Journal of Membrane Science 2018; 567: 157-65. https://doi.org/10.1016/j.memsci.2018.09.003
[83] Quilaqueo M, Aguilera JM. Crystallization of NaCl by fast evaporation of water in droplets of NaCl solutions. Food Research International 2016; 84(2): 143-9. https://doi.org/10.1016/j.foodres.2016.03.030